



Scaffold Searching of FDA and EMA-Approved Drugs Identifies Lead Candidates for Drug Repurposing in Alzheimer's Disease

Sergey Shityakov^{1*}, Ekaterina V. Skorb^{1*}, Carola Y. Förster² and Thomas Dandekar^{3*}

¹Laboratory of Chemoinformatics, Infochemistry Scientific Center, ITMO University, Saint-Petersburg, Russia, ²Department of Anaesthesiology, Intensive Care, Emergency and Pain Medicine, Würzburg University Hospital, Würzburg, Germany, ³Department of Bioinformatics, Biocenter, University of Würzburg, Würzburg, Germany

OPEN ACCESS

Edited by:

Aleksey E. Kuznetsov,
Federico Santa María Technical
University, Chile

Reviewed by:

Uttam Pal,
S.N. Bose National Centre for Basic
Sciences, India
Weiwei Han,
Jilin University, China

*Correspondence:

Sergey Shityakov
shityakoff@hotmail.com
Ekaterina V. Skorb
skorb@itmo.ru
Thomas Dandekar
dandekar@biozentrum.uni-
wuerzburg.de

Specialty section:

This article was submitted to
Theoretical and Computational
Chemistry,
a section of the journal
Frontiers in Chemistry

Received: 05 July 2021

Accepted: 22 September 2021

Published: 22 October 2021

Citation:

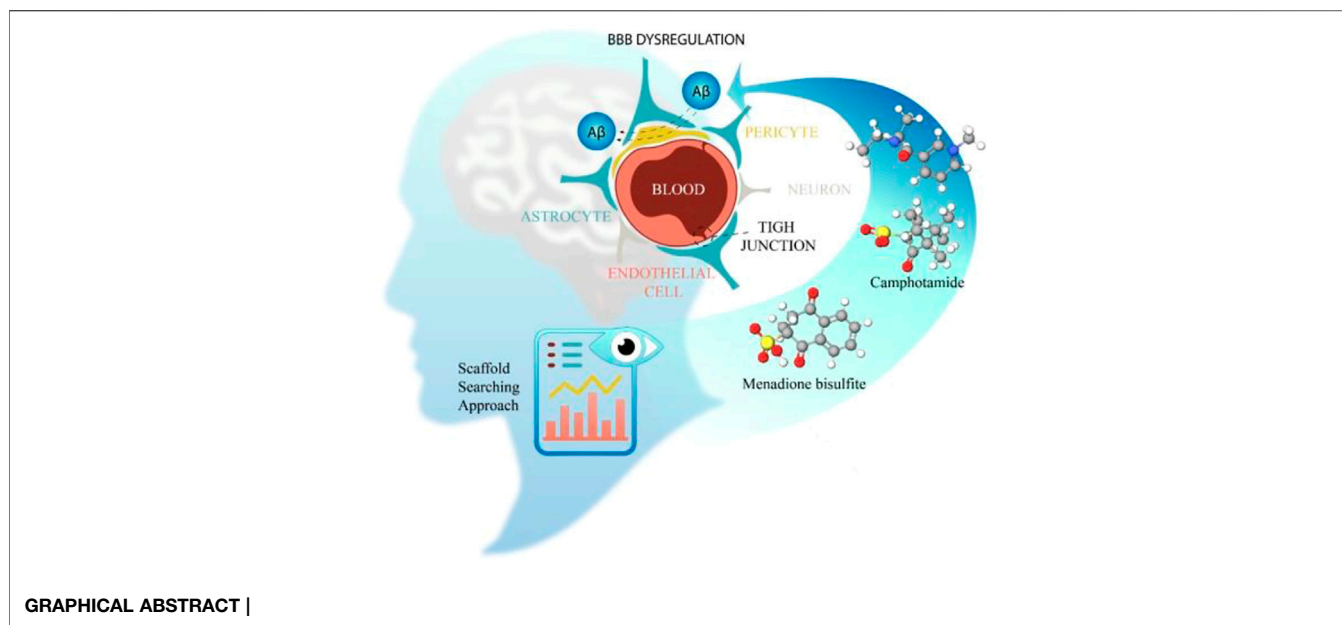
Shityakov S, Skorb EV, Förster CY and
Dandekar T (2021) Scaffold Searching
of FDA and EMA-Approved Drugs
Identifies Lead Candidates for Drug
Repurposing in Alzheimer's Disease.
Front. Chem. 9:736509.
doi: 10.3389/fchem.2021.736509

Clinical trials of novel therapeutics for Alzheimer's Disease (AD) have consumed a significant amount of time and resources with largely negative results. Repurposing drugs already approved by the Food and Drug Administration (FDA), European Medicines Agency (EMA), or Worldwide for another indication is a more rapid and less expensive option. Therefore, we apply the scaffold searching approach based on known amyloid-beta (A β) inhibitor tramiprosate to screen the DrugCentral database ($n = 4,642$) of clinically tested drugs. As a result, menadione bisulfite and camphotamide substances with protrombogenic and neurostimulation/cardioprotection effects were identified as promising A β inhibitors with an improved binding affinity (ΔG_{bind}) and blood-brain barrier permeation (logBB). Finally, the data was also confirmed by molecular dynamics simulations using implicit solvation, in particular as Molecular Mechanics Generalized Born Surface Area (MM-GBSA) model. Overall, the proposed *in silico* pipeline can be implemented through the early stage rational drug design to nominate some lead candidates for AD, which will be further validated *in vitro* and *in vivo*, and, finally, in a clinical trial.

Keywords: scaffold search, approved drugs, drug repurposing, alzheimer's disease, chemical similarity, molecular modeling

INTRODUCTION

Alzheimer's Disease (AD) is a progressive neurodegenerative disorder, causing memory loss and in 60–70% of cases leading to dementia (Caltagirone et al., 1983). The AD pathology is widely believed to be associated with the production of β -amyloid peptide (A β), which is responsible for the plaque formations in the brain, disrupting normal neuronal functions (Takahashi et al., 2017). This pathological hallmark of AD might be considered in rational drug design and discovery as a promising therapeutic target to develop effective medication against this disorder. However, there is still a lack of efficient treatment for this disabling and ultimately fatal disease, e.g., donepezil and memantine usually provide at best only temporary and



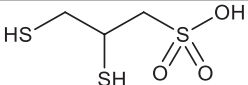
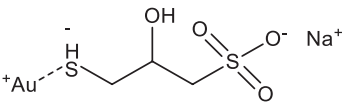
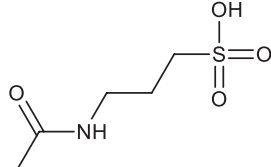
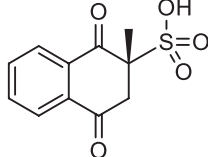
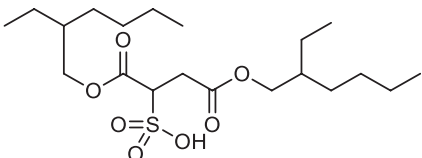
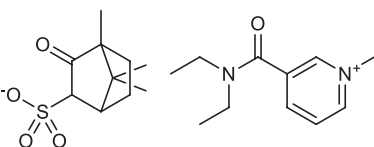
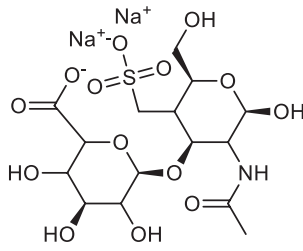
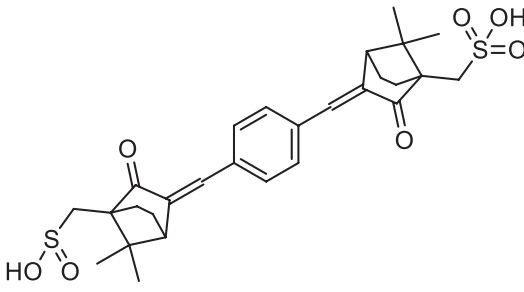
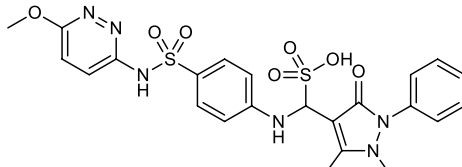
incomplete symptomatic relief (Nie et al., 2011). Moreover, various attempts had been made to use different drug binding sites (subregion-targets) in A β that could stop its aggregation and formation of a senile plaque (Nie et al., 2011). In particular, tramiprosate (3-Aminopropanesulfonic acid, TRA), a mimic of glycosaminoglycans, targets the HHQK subregion at the N-terminus of A β (Nie et al., 2011). The TRA treatment of TgCRND8 mice resulted in a 30% reduction in the brain plaque load and the same decrease in the cerebral levels of soluble and insoluble A β (Gervais et al., 2007). Additionally, a dose-dependent 60% reduction of plasma A β levels was also observed, suggesting that this influences the A β central pool, changing either its efflux or its metabolism in the brain (Gervais et al., 2007). Despite the structural simplicity, high specificity, and excellent *in vivo* A β inhibition properties of TRA, it subsequently failed in the late stages of phase III clinical trial (Rauk, 2008). However, the data obtained from *in vitro/vivo* experiments and clinical trials could provide valuable evidence that A β inhibitors and their scaffolds represent a viable drug designing methodology for AD treatment (Blazer and Neubig, 2009). Indeed, some scaffold-based techniques, such as scaffold hopping, have become a powerful tool to determine the most promising drug-like candidates and already approved drugs in a drug repurposing protocol for AD (Kowal et al., 2019; Ballard et al., 2020). For example, some researchers had already performed *in silico* screening of a virtual library of a biaryl scaffold-containing compounds to inhibit the primary targets of AD therapeutics, such as acetylcholinesterase, β -secretase, monoamine oxidases, and N-methyl-D-aspartate receptor (Khalid et al., 2018). On the other hand, the scaffold searching of FDA and EMA-approved drug libraries was not previously performed to identify lead candidates for drug repurposing in AD. Moreover, the blood-brain Barrier (BBB) permeation of drug-like molecules is often considered in various pharmacokinetics (PK) studies as a pivotal PK-related descriptor (Shityakov et al., 2012; Carpenter et al., 2014). Therefore, in our study, we wanted to apply the molecular search based on the TRA

scaffold to examine a database of FDA and EMA-approved drugs using *in silico* computational approaches, such as virtual screening, molecular dynamics, and BBB-based descriptor analyses.

COMPUTATIONAL METHODS

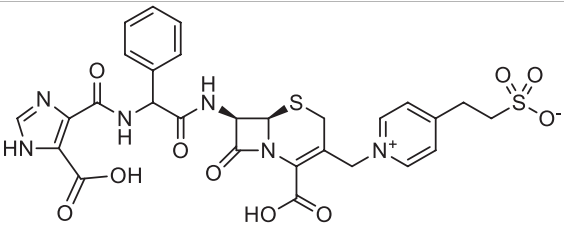
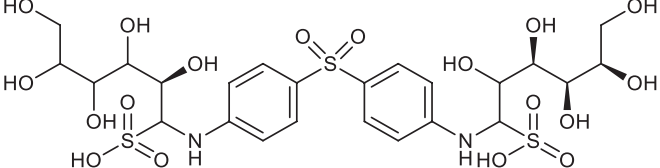
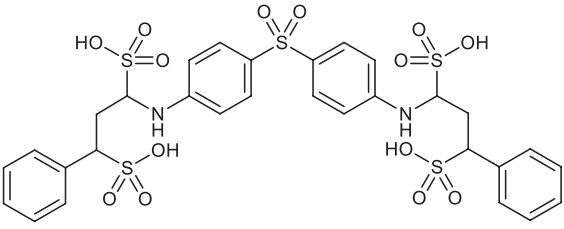
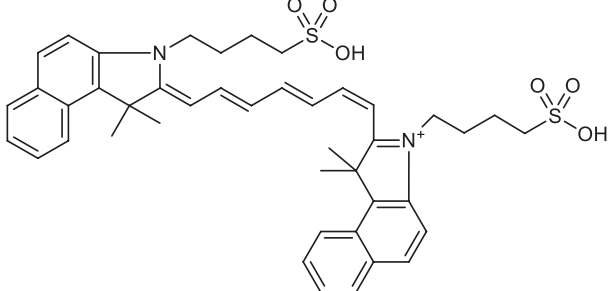
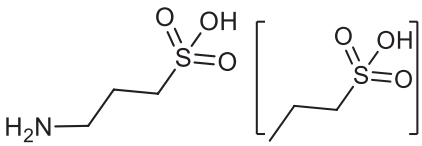
The 3D molecular structure (PDB ID: 2NAO) of a disease-relevant A β fibril (1–42), containing chains A, B, and C, was downloaded from the Protein Data Bank (Walti et al., 2016) to be used in the study. The Ramachandran plot server (<https://zlab.umassmed.edu/bu/rama/index.pl>) was implemented for the stereochemical validation of the receptor molecule to investigate the ϕ - ψ dihedral angles in a Ramachandran plot. Altogether, observed statistics showed that 86.54% (90 residues) and 11.54% (12 residues) of all observed residues were in the core and allowed regions. Additionally, no steric clashes were detected in the peptide structure. The TRA molecule and its propanesulfonic scaffold were built by using the MarvinSketch software (ChemAxon, Hungary). A database, containing the FDA and EMA-approved drugs ($n = 4,642$), was obtained from the DrugCentral 2021 online drug compendium. The Molsoft ICM 3.8-3 scaffold search algorithm was used to filter the database to identify scaffold-containing drugs. All ligands were protonated at pH = 7.4 and T = 310 K using the MOE software. Prior to molecular docking, the CASTp (Computed Atlas of Surface Topology of proteins) algorithm (Naghizadeh, 2001) was implemented to detect the location of the peptide-ligand binding site with Cartesian coordinates located at the grid center: $x = 11.87 \text{ \AA}$; $y = 18.88 \text{ \AA}$; $z = -27.75 \text{ \AA}$. The AutoDock molecular docking algorithm to calculate binding affinity (ΔG_{bind}) was implemented via the Raccoon v1.0 modeling suite to perform virtual screening. The receptor and ligand structure preparations for molecular docking included Gasteiger partial charges assignment and rotatable bonds definition according to the standard protocol published elsewhere (Shityakov et al., 2014). The inhibition

TABLE 1 | Chemical structures and clinical indications of FDA and EMA-approved drugs ($n = 13$) containing propanesulfonic scaffold of TRA.

Compound	Structure	Indication
1. Unithiol		Mercury, arsenic, and lead poisoning
2. Aurotioprol		Moderate-severe rheumatoid arthritis and tuberculosis
3. Acamprosate		Abstinence from alcohol
4. Menadione		Hypoprothrombinemia
5. Docusate sodium		Occasional constipation
6. Camphotamide		Cardioprotection and neurostimulation
7. Dermatan sulfate		Deep vein thrombosis
8. Ecamsule		Skin protection
9. Sulfamazole		Sulfonamide antibiotic with antipyretic properties

(Continued on following page)

TABLE 1 | (Continued) Chemical structures and clinical indications of FDA and EMA-approved drugs ($n = 13$) containing propanesulfonic scaffold of TRA.

Compound	Structure	Indication
10. Cefpimizole		Infections of skin or soft tissue and urinary tract
11. Glucosulfone		Treatment of malaria tuberculosis and leprosy
12. Solasulfone		Treatment of leprosy
13. Indocyanine green		Ophthalmic angiography and treatment of cancer and acne vulgaris
14. TRA [scaffold]		AD (failed in phase III)

constants (K_i) and Ligand Efficiencies (LE) were calculated from the binding energy values as follows:

$$K_i = \exp\left[\frac{\Delta G_{bind}}{RT}\right]$$

$$LE = \frac{\Delta G_{bind}}{N_{atm}}$$

where R (gas constant) is $1.98 \text{ cal}(\text{mol} \cdot \text{K})^{-1}$; T (room temperature) is 298.15 K ; N_{atm} is the number of non-hydrogen atoms in a molecule. AutoDock v.4.2.5.1 was used in the study since its previous version incorrectly calculates part of the intermolecular desolvation energy term (Goodsell et al., 1996). The docking grid with dimension size of

$60 \times 60 \times 60 \text{ \AA}$ and a grid spacing of 0.375 \AA were used in the study. The Glide molecular docking algorithm with the Prime MM-GBSA (generalized Born solvent-accessible surface area) approach to calculate the free energy of binding (ΔG_{PR}) was implemented using the default settings, such as the OPLS3e force field, 0.25 of charge cutoff, and 0.8 scaling of the vdW radii of non-polar receptor and ligand atoms. The G-score value, as an empirical scoring function, was used to approximate the ligand binding free energy. All molecular dynamics (MD) simulations were performed using the AMBER 16 package with the FF99SB and GAFF force fields for the A β peptide and its ligands (Case et al., 2005). The Antechamber module of AmberTools was employed to calculate the partial charges of the ligands using the semi-empirical AM1-BCC function according to the

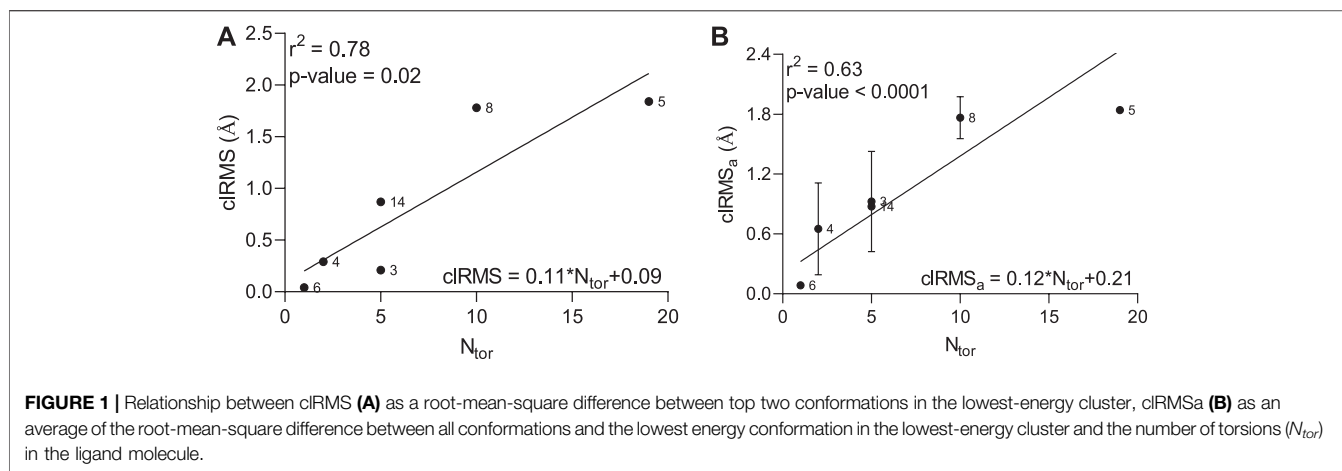


TABLE 2 | Summary of AutoDock molecular docking results for drugs ($n = 13$), containing propanesulfonic scaffold of TRA.

Compound	ΔG_{bind} kcal/mol	cIRMSD Å	cIRMSD _a Å	N_{atm}	N_{tor}	Ki μ M	LE	T
1	-3.05	—	—	12	6	5.7 ^a	-0.25	0.57
2	-3.7	—	—	11	5	1.89 ^a	-0.34	0.67
3	-5.15	0.21	0.74	13	5	162.66	-0.39	0.71
4	-7.11	0.29	0.54	18	2	5.87	-0.39	0.56
5	-4.97	1.84	1.84	29	19	220.65	-0.17	0.63
6	-6.82	0.04	0.07	15	1	9.61	-0.46	0.5
7	-4.26	—	—	37	12	734.58	-0.12	0.56
8	-6.17	1.78	1.18	40	10	28.9	-0.15	0.45
9	-5.91	—	—	41	10	44.89	-0.14	0.33
10	-2.97	—	—	52	15	6.53 ^a	-0.06	0.27
11	0.66	—	—	61	30	3.06 ^b	0.01	0.44
12	-3.81	—	—	57	20	1.57 ^a	-0.07	0.44
13	-5.71	—	—	55	16	62.99	-0.1	0.42
14	-6.19	0.87	0.58	11	5	27.94	-0.56	0.67

^amM.

^bM.

standard protocol (Marques et al., 2021). The systems were solvated with the TIP3P water models and neutralized by adding the Na⁺ ions using the tLEap input script available from the AmberTools package. Long-range electrostatic interactions were modeled via the particle-mesh Ewald method (Essmann et al., 1995). The SHAKE algorithm (Miyamoto and Kollman, 1992) was applied to constrain the length of covalent bonds, including the hydrogen atoms. Langevin thermostat was implemented to equilibrate the temperature of the system at 310 K. A 2.0-fs time step was used in all of the MD setups. For the minimization and equilibration (NVT and NPT ensembles) phases, 100,000 steps and a 1-ns period were used, respectively. Finally, 100-ns classical MD simulations, with no constraints as NPT ensemble, were performed for each of the peptide-ligand complexes using the molecular mechanics combined with the Poisson-Boltzmann (MM-PBSA) or generalized Born (MM-GBSA) augmented with the hydrophobic solvent-accessible surface area term (Kollman et al., 2000; Shityakov et al., 2017). The MM-PBSA/GBSA solvation models were applied as a post-processing end-state method to calculate the free energies

(ΔG_{PB} and ΔG_{GB}) together with the entropies ($T\Delta S$) and enthalpies (ΔH) for the analyzed molecules, namely:

$$\Delta G_{PB} = \Delta H_{PB} - T\Delta S; \Delta G_{GB} = \Delta H_{GB} - T\Delta S$$

To calculate the blood-brain barrier partitioning coefficients ($\log BB$), the in-house python script, based on the Clark ($\log BB_{cl}$) and Rishton ($\log BB_{ri}$) linear regression models, was ran according to the following equations (Clark, 2003; Rishton et al., 2006):

$$\log BB_{cl} = 0.152AlogP - 0.0148PSA + 0.139$$

$$\log BB_{ri} = 0.155AlogP - 0.01PSA + 0.164$$

where PSA and $AlogP$ are the polar surface area and atom-based octanol-water partitioning coefficient. The in-house PyMol script was applied to calculate the Buried Surface Area (BSA) of the peptide-ligand complexes according to the equation:

$$BSA = \frac{(ASA_{pep} + ASA_{lig}) - ASA_{comp}}{2}$$

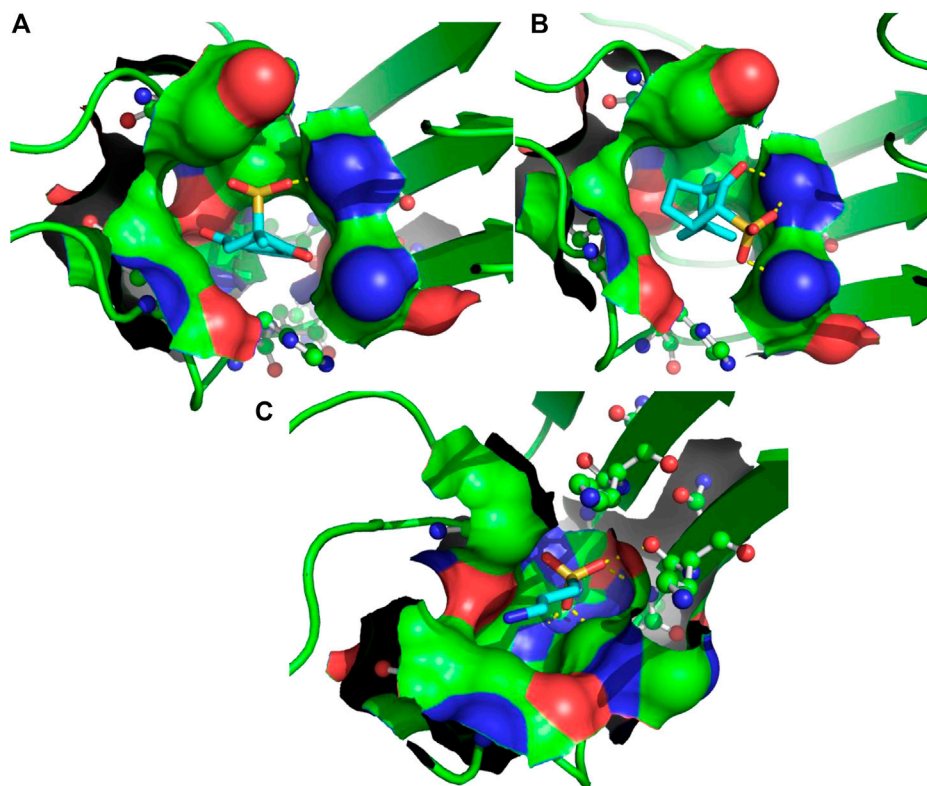


FIGURE 2 | 3D binding modes predicted from the AutoDock runs for menadione (A), camphotamide (B), and TRA (C) bound to A β peptide. The peptide-ligand binding site is shown by the molecular surface and colored according to the peptide atomic composition. The peptide is shown as a ribbon diagram, and its residues are drawn as ball-and-stick models. Hydrogen bonds are visualized as a dashed lines. The ligand molecules are depicted in sticks, and hydrogen atoms are removed to enhance clarity.

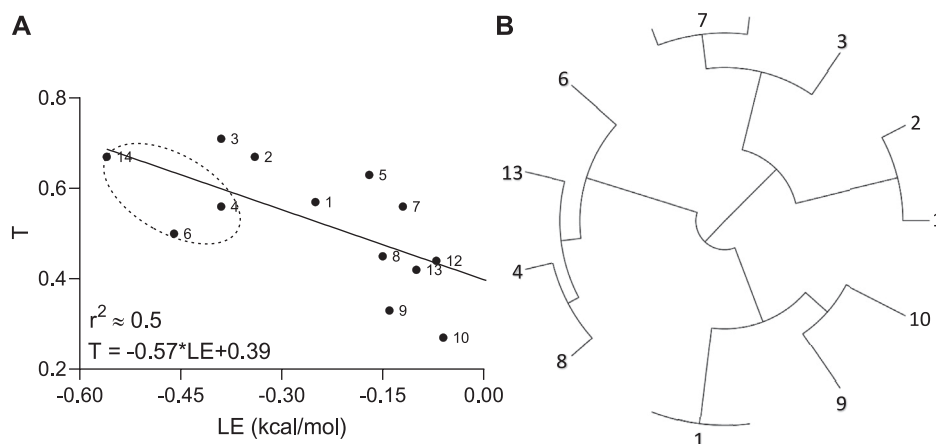


FIGURE 3 | Relationship (A) between Tanimoto similarity (T) and ligand efficiency (LE) descriptors and tree visualization (B) of the hierarchical clustering based on structural similarities calculated for hit molecules ($n = 13$), containing propanesulfonic scaffold of TRA.

where ASA_{pep} and ASA_{lig} and ASA_{comp} are the accessible surface areas of the peptide, ligand, and complex components. Molecular descriptors, such as molecular weight (MW), $AlogP$, H-bond acceptors (HBA), H-bond donors (HBD), PSA , quantitative

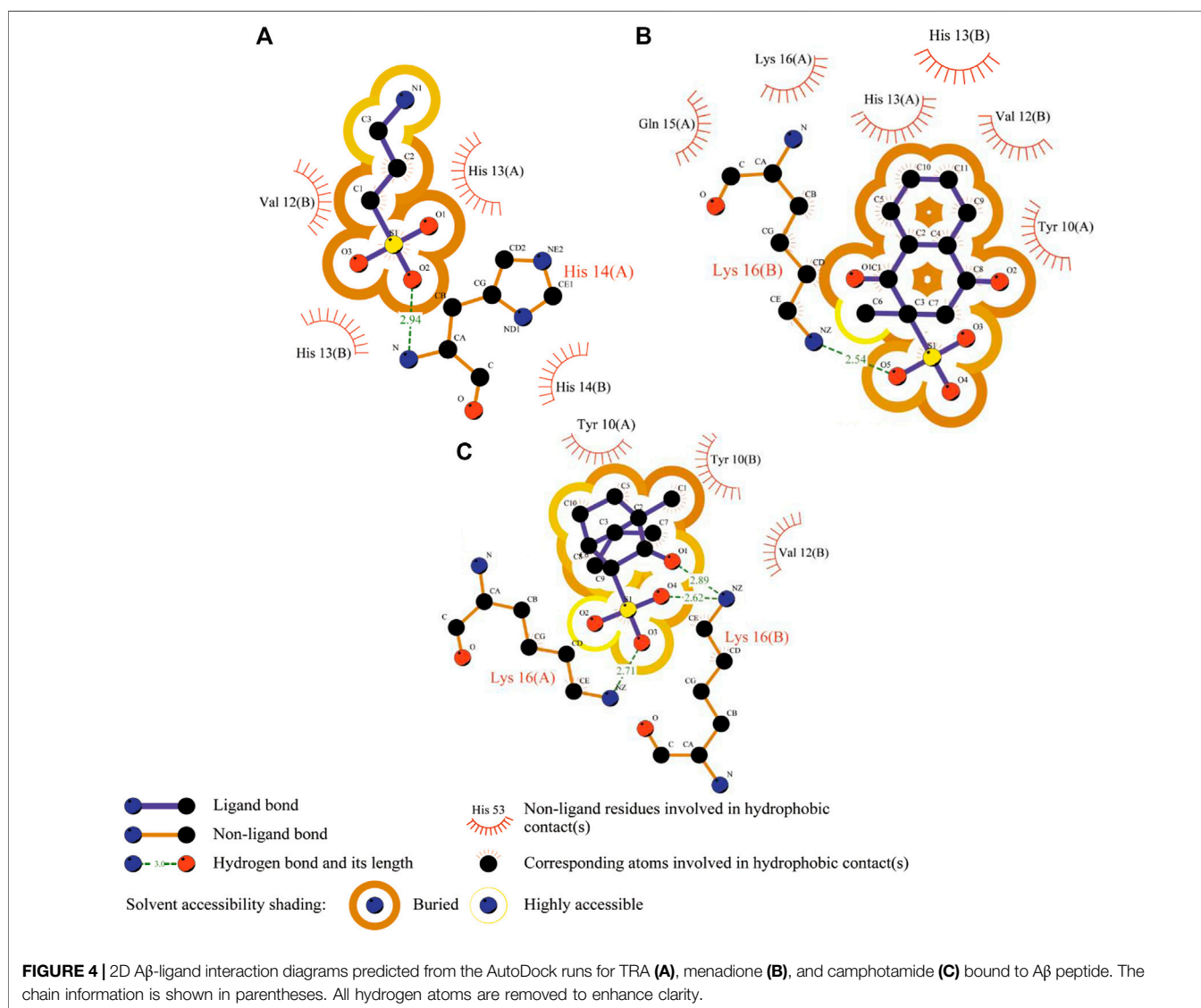
estimate of drug-likeness (QED), and Tanimoto molecular similarity (T) indexes were calculated with the Biscu-it™ tools and Rcp1 and Rcdk libraries within the *Python* and *R* environments (Voicu et al., 2020; Cao et al., 2015). Buried surface areas (BSA)

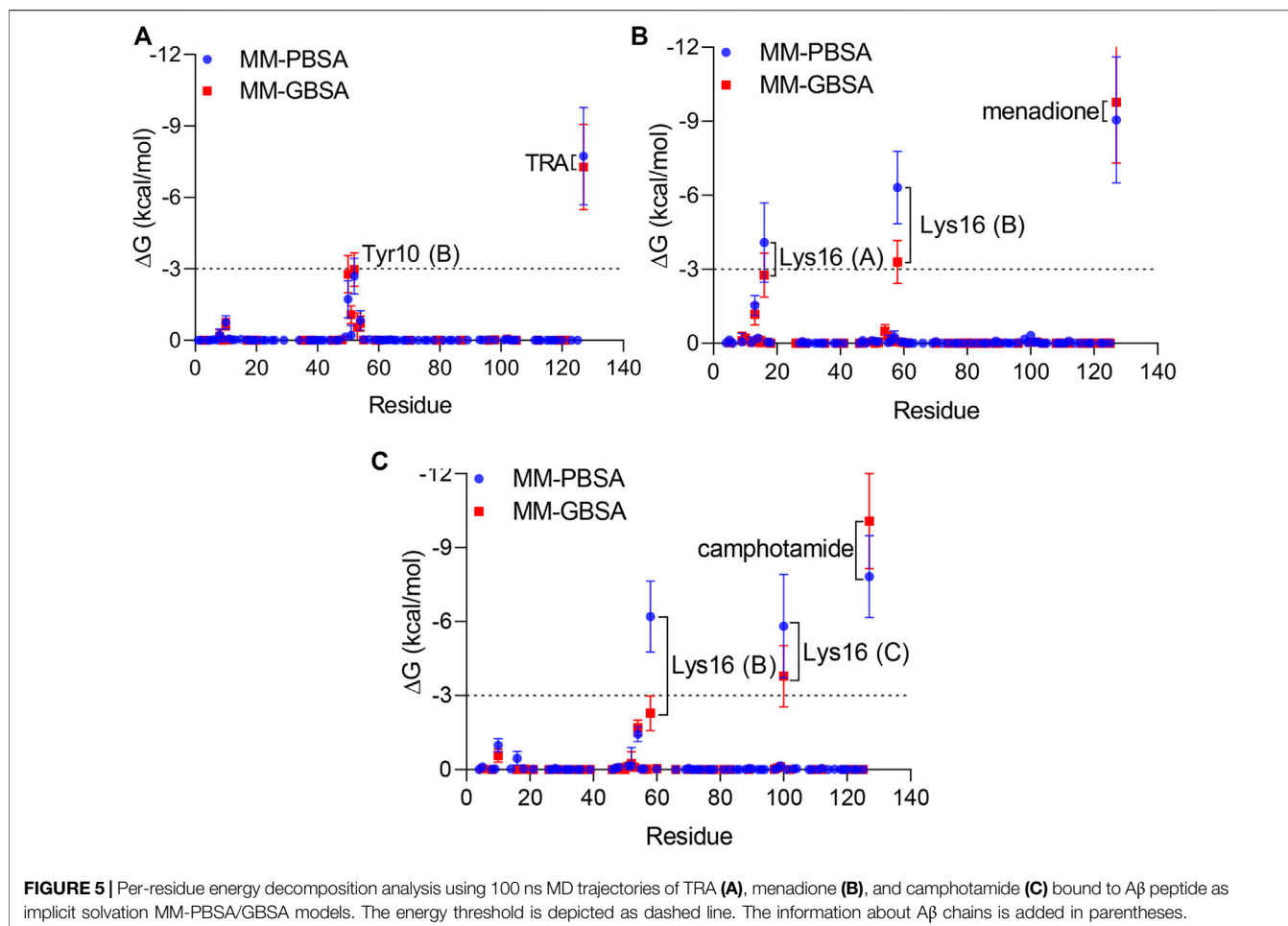
TABLE 3 | Summary of molecular descriptors and partitioning coefficients ($\log BB$) determined for lead compounds (drugs) with highest A β inhibition properties.

Compound	MW	AlogP	HBA	HBD	PSA	QED	$\log BB_{Cl}$	$\log BB_{Hi}$	$\log BB_{exp}$
Menadione	253.25	0.98	4	0	88.18	0.76	-1.02	-0.57	—
Camphotamide	231.29	1.14	3	0	71.11	0.69	-0.74	-0.37	—
TRA	138.17	-0.91	3	1	80.06	0.58	-1.18	-0.78	—
Donepezil	379.5	4.36	4	0	38.77	0.72	0.23	0.45	0.89

TABLE 4 | Summary of binding affinities (ΔG and G-score), entropy ($T\Delta S$), enthalpy (ΔH_{PB} and ΔH_{GB}), and Buried Surface Area (BSA) values calculated for lead candidates and TRA. Entropy-enthalpy compensation data of the peptide-ligand complexes is obtained from the normal-mode analyses of 100 ns trajectories at the temperature of 298.15 K.

Compound	ΔG_{PB}	ΔG_{GB}	ΔG_{PR}	G-score kcal/mol	$T\Delta S$	ΔH_{PB}	ΔH_{GB}	BSA, Å ²
Menadione	-13.75	-19.71	-38.81	-6.51	-20.4	-34.15	-40.11	489.77
Camphotamide	-15.61	-14.86	-21.36	-5.08	-17.86	-33.47	-32.72	481.09
TRA	-2.28	-10.1	-16.31	-4.49	-17.91	-20.19	-28.01	373.56





have been calculated for 2D A β -ligand interaction diagrams using the NACCESS program (Hubbard and Thornton, 1993; Wallace et al., 1995). Molecular graphics and visualization were performed with the LigPlot + program (EMBL-EBI, Wellcome Trust Genome Campus, Hinxton, United Kingdom) in order to build two-dimensional interaction diagrams from three-dimensional coordinates. Linear regression analysis, followed by graphical representation was performed by PyMol and GraphPad Prism v.8 (GraphPad Software, San Diego, CA, United States). The differences were considered statistically significant at a p -value of <0.05 .

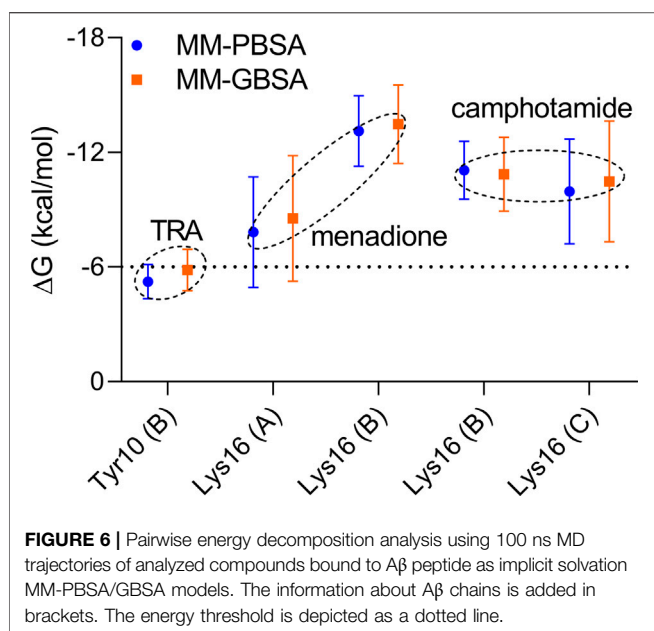
RESULTS AND DISCUSSION

Before molecular docking and MD simulations, the DrugCentral database ($n = 4,642$) was filtered to find the molecules, containing the propanesulfonic scaffold of TRA. The scaffold search protocol is based on the chemical similarity searching that can be used to screen a database of compounds for structural similarity to a query chemical structure. The small portion ($n = 13$) of FDA and EMA-approved drugs (Table 1), containing propanesulfonic scaffold of TRA, was identified as several hit molecules

suitable for further investigation using molecular docking to eventually locate some lead candidates. In fact, our study relies on the modified hit-to-lead protocol to identify promising lead compounds, inhibiting A β in order to highlight the possibility for their optimization.

The identified hit molecules belong to different chemical classes and can be prescribed to treat various pathological conditions, such as bacterial infections (leprosy and tuberculosis), lead or mercury poisoning, metabolic disorders, and neurological conditions. Subsequently, the rigid-flexible molecular docking was performed to calculate the affinity between hit substances and A β , targeting the HHQK subregion at the N-terminus of the peptide. The lowest-energy A β conformer of the NMR models ($n = 10$) was chosen as a receptor molecule for molecular docking with the potential energy of $-1,106.70$ kcal/mol, which makes it more stable in the solution. Additionally, the 3D alignment of the A β peptide and HHQK region revealed the 2.0 Å structural deviation indicating a relatively “conserved” protein-receptor binding site in solution NMR models (Supplementary Figures S1A,B).

To accurately assess any correlations between the number of atoms in the ligand molecule and the conformational effects happening within the peptide-ligand binding site, we estimated



the root-mean-square (*RMS*) difference between the top two conformations and its average value calculated between all conformations and the lowest-energy conformation in the lowest-energy cluster (**Supplementary Figure S2**). A strong positive correlation ($r^2 = 0.78$) with reliable statistics (p -value = 0.02) between the *clRMS*, as an *RMS* difference between top two conformations in the largest cluster, and the number of torsions (N_{tor}) was observed by linear regression analysis (**Figure 1A**). Furthermore, a significant standard deviation of the *clRMS* variable, as an average of the *RMS* difference between all conformations and the lowest energy conformation, was detected for some hit compounds (3, 4, 8, and 14), describing the elevated conformational change (**Figure 1B**), which greatly affects the correlation coefficient ($r^2 = 0.63$).

Finally, menadione and camphotamide lead candidates were found among the top binders (**Table 2** and **Figures 2A,B**) with the binding energy values (-7.11 and -6.82 kcal/mol) significantly lower than for the reference compound with a ΔG_{bind} value of -6.19 kcal/mol (**Table 2** and **Figure 2C**). It was previously published that menadione sodium bisulfite as a remedy against hemorrhagic disease caused by vitamin K deficiency could inhibit A β toxic formation and aggregation in *C. elegans*, extending its life span and reducing disruption of cellular membranes (Zhang et al., 2018). The co-authors also hypothesized that menadione might inhibit amyloid formation due to its backbone similarity to 1,4-naphthoquinone, which shows strong anti-aggregation effects on amyloidogenic proteins, such as insulin and α -synuclein. Similarly, the 6-hydroxy-nicotine intermediate from *P. nicotinovorans* as a precursor for camphotamide has been shown to have neuroprotective effects with putative applications in AD treatment (Wang et al., 2015; Hritcu et al., 2017). As a positive inotropic agent (cardiotonic), this substance could be potentially prescribed to treat AD-associated amyloid cardiomyopathy, inhibiting, directly and indirectly, A β accumulation in the heart.

Indeed, the inhibition of A β and the formation of neurofibrillary tangles along the heart-brain axis could be reached through targeted supplementation of neurotrophic factors to the brain as it was hypothesized by Shityakov and coauthors Shityakov et al. (2021).

To investigate how molecular similarity contributes to the A β binding, the Tanimoto coefficients as an appropriate choice for a fingerprint-based similarity and ligand efficiency as the affinity normalized by the number of non-hydrogen atoms were implemented. A moderate negative correlation ($r^2 \approx 0.5$) with reliable statistics (p -value = 0.008) between the *T* and *LE* parameters was observed by linear regression analysis (**Figure 3**).

In other words, if chemical compounds match more to the TRA scaffold, they also have very similar binding modes calculated per number of heavy atoms in the molecule. In addition, all hit molecules were subdivided into 4 big groups or clusters by the hierarchical clustering according to their E-state molecular fingerprints and pairwise similarity matrix, where the lead molecules (compounds 4 and 6) ended up in the same cluster (**Figure 3B**).

Next, the *AlogP*, *QED*, *PSA*, and *logBB* values for menadione, camphotamide, and TRA as a reference, and donepezil as standard control were calculated to evaluate the drug ability to possess the optimal BBB permeation properties and druglikeness (**Table 3**).

The *AlogP* parameter for lead candidates suggested their mild lipophilic properties, which were significantly higher than for the reference substance but not as good as for the standard control. On the other hand, the *QED* parameters for lead candidates were very similar to those determined for donepezil, reflecting the distribution of molecular properties, such as the number of hydrogen bond donors and acceptors, the number of aromatic rings, and the presence of unwanted chemical functionalities. However, for a CNS-active compound to permeate the BBB, a surface area less than $60\text{--}70 \text{ \AA}^2$ is usually required to achieve the desired brain bioavailability for the administered drug (Shityakov et al., 2014; Kelder et al., 1999). Judging by relatively low *AlogP* and high *PSA*, there is a risk that the BBB permeation of the lead candidates might not be entirely sufficient as confirmed by the *logBB*, which optimally should be $\logBB > 0$ (Shityakov et al., 2015). Therefore, further lead optimization by *in situ* enumeration or fragment replacement might be a plausible choice to make chemical modifications, improving brain bioavailability (*logBB*) together with selectivity, pharmacokinetic and pharmacodynamic parameters, and decreasing toxicity. Reaction-based *in situ* enumeration can be achieved by proposing synthetically feasible candidates from a reagent library in particular, which reagents are most likely to produce potential active compounds for the binding site (Mok et al., 2017). On the contrary, the fragment replacement protocol performs scaffold hopping by replacing part of the scaffold structure while maintaining the favorable binding between the receptor and the ligand (Vainio et al., 2013). The elevated experimental *logBB* index of 0.89 for donepezil was mainly due to its carrier-mediated transport to the brain (Kim et al., 2010). It could probably be accomplished by organic cation or choline transporters (OCT1-3 and CHT1) and not just crossing the BBB via passive diffusion through endothelial cells (Kim et al., 2010).

To validate further molecular docking results, the free energy of binding based on implicit solvation models was calculated for amyloid-drug complexes. The MM-PBSA/GBSA calculations (Table 4), using 100 ns MD trajectories, confirmed the previous data completely (GBSA) and partially (PBSA), revealing much higher binding affinities of lead compounds to A β in comparison to the reference.

The former protocol provided the best affinity for menadione ($\Delta G_{GB} = -19.71$ kcal/mol), probably because in some extensive studies the MM-GBSA approach was computationally more efficient, achieving better accuracy but being less rigorous (Hou et al., 2011). Therefore, the second validation was done to clarify the MM-PBSA/GBSA discrepancy by utilizing the Prime algorithm with the MM-GBSA-based scoring function. As a result, the G-score data and the entropy-enthalpy compensation analysis confirmed the previous findings, describing the exothermic nature ($\Delta H < 0$) of the binding process with the decreased disorder ($T\Delta S < 0$), which could occur spontaneously depending on temperature. Additionally, the BSA values (Table 4 and Figures 4A–C), which measures the size of the A β -drug interface, also confirmed the previous binding affinity pattern, where the BSA elevation leads to an increase in binding as it was already published for the peptide-ligand and host-guest systems (Shityakov et al., 2020; Esmaeilpour et al., 2021).

To analyse the movements of the studied complexes, the root-mean-square deviation (RMSD) and fluctuation (RMSF) values together with the radius of gyration (R_g) with respect to the initial conformation were plotted versus time (Supplementary Figures S3A–E). The receptor RMSD values were relatively high (RMSD = 10 Å) stabilized after about 20 ns for the compound 4 and 6/A β complexes and after 40 ns for TRA/A β (Supplementary Figure S3A). The ligand RMSD remained low within 1.0 Å and stabilized almost instantly (Supplementary Figure S3B). The receptor RMSF values produced some picks associated with the high flexibility of the A β termini (Supplementary Figure S3C). The atomic fluctuations of ligands showed more stable profiles especially for compounds 4 and 6 (Supplementary Figure S3D). The decreased R_g values were associated with the receptor compactness, which was elevated during the simulation (Supplementary Figure S3E). Finally, the number of H-bonds between the receptor and its ligands and the fraction of residues involved in H-bonding were assessed to find the H-binding contribution to the affinity. These parameters were the highest for compound 4 with more H-bonds formed, (Supplementary Figure S3F) significantly increasing the residue fraction (Supplementary Figure S3G).

Finally, per-residue and pairwise energy decomposition analyses were employed to evaluate the energetic contribution of drugs and the binding site residues. Some unique residues, such as Tyr10 (B) for TRA, Lys16 (A, B) for menadione, and Lys16 (B, C) for camphotamide were identified at the energetic threshold ($\Delta G = -3.0$ kcal/mol) and below by one or both implicit solvation protocols (Figures 5, 6). In particular, all amino acid residues involved in the interaction with the lead candidates had exceeded the energetic threshold (Figure 5A,B), which was not observed for the reference molecule (Figure 5C). Meanwhile, the Lys16 targeting in A β by the oxidation of a catechol structure to the *o*-quinone forming the *o*-quinone-A β adduct is believed to be responsible for its anti-aggregation activity (Liu et al., 2017).

In the pairwise interaction, only Tyr10 (B) was detected slightly above the adjusted energetic threshold ($\Delta G = -6.0$ kcal/mol), and Lys16 (B) had the lowest energy during the MD simulation of the A β -menadione complex (Figure 6). Highlighting the contribution of these residues for the inhibitor of this site, curcumin and resveratrol were found to interact with Arg5, Ser8, Tyr10, Gln15, Lys16, Leu17, and Phe20 (Fu et al., 2014). Besides, solvent-accessible residues, such as Phe20 at the N-terminal.

KLVFF stretch was reported as crucial in the interactions of these two inhibitors (Fu et al., 2014). Some studies have also documented the pairwise interactions for some amyloid variants (A β_{10-35}) to illustrate residue energetic contributions in a process of A β reorganization driven basically by inter-chain hydrophobic and hydrophilic interactions and also solvation/desolvation effects (Campanera and Pouplana 2010).

CONCLUSION

In this study, the scaffold searching approach based on known A β inhibitor tramiprosate to screen the DrugCentral database ($n = 4,642$) was employed to identify hit compounds ($n = 13$) and lead candidates ($n = 2$) for AD drug repurposing. Two lead candidates, namely menadione bisulfite and camphotamide, out of 13 hit compounds were identified as promising A β inhibitors with the improved ΔG_{bind} and $logBB$ parameters. The binding affinity modes were also confirmed by molecular dynamics simulations using implicit solvation models, in particular MM-GBSA. We assume that this scaffold searching methodology in conjunction with pharmaceutical profiles ($logBB$) can be applied as a starting routine for drug repurposing in AD. Overall, the proposed computational pipeline can be implemented through the early stage rational drug design to nominate drugs for AD that, after additional *in vitro* and *in vivo* validation, could be readily evaluated in a clinical trial.

DATA AVAILABILITY STATEMENT

The original contributions presented in the study are included in the article/Supplementary Material, further inquiries can be directed to the corresponding authors.

AUTHOR CONTRIBUTIONS

SS, ES, CF, and TD conceptualized the topic. SS performed the experiments and wrote the manuscript. All co-authors read the manuscript. All authors contributed to the article and approved the submitted version.

ACKNOWLEDGMENTS

Special thanks are extended to Todd Axel Johnsen from the Infochemistry Scientific Centre, ITMO University for his assistance

in the editing and proofreading of the manuscript. ITMO Fellowship Professorship Program and Goszadanie no. 2019-1075 are acknowledged for the support. TD acknowledges the Land of Bavaria for its contribution to the DFG project 324392634-TRR 221/INF and DFG project 374031971-TRR 240/INF.

REFERENCES

- Ballard, C., Aarsland, D., Cummings, J., O'Brien, J., Mills, R., Molinuevo, J. L., et al. (2020). Drug Repositioning and Repurposing for Alzheimer Disease. *Nat. Rev. Neurol.* 16 (12), 661–673. doi:10.1038/s41582-020-0397-4
- Blazer, L. L., and Neubig, R. R. (2009). Small Molecule Protein-Protein Interaction Inhibitors as CNS Therapeutic Agents: Current Progress and Future Hurdles. *Neuropsychopharmacology* 34 (1), 126–141. doi:10.1038/npp.2008.151
- Caltagirone, C., Albanese, A., Gainotti, G., and Masullo, C. (1983). Acute Administration of Individual Optimal Dose of Physostigmine Fails to Improve Mnesic Performances in Alzheimers Presenile Dementia. *Int. J. Neurosci.* 18 (1-2), 143–147. doi:10.3109/00207458308985888
- Campanera, J. M., and Pouplana, R. (2010). MMPBSA Decomposition of the Binding Energy throughout a Molecular Dynamics Simulation of Amyloid-Beta (Aβeta(10-35)) Aggregation. *Molecules (Basel, Switzerland)* 15 (4), 2730–2748. doi:10.3390/molecules15042730
- Cao, D.-S., Xiao, N., Xu, Q. S., and Chen, A. F. (2015). Rcpic: R/Bioconductor Package to Generate Various Descriptors of Proteins, Compounds and Their Interactions. *Bioinformatics (Oxford, England)* 31 (2), 279–281. doi:10.1093/bioinformatics/btu624
- Carpenter, T. S., Kirshner, D. A., Lau, E. Y., Wong, S. E., Nilmeier, J. P., and Lightstone, F. C. (2014). A Method to Predict Blood-Brain Barrier Permeability of Drug-like Compounds Using Molecular Dynamics Simulations. *Biophysical J.* 107 (3), 630–641. doi:10.1016/j.bpj.2014.06.024
- Case, D. A., Cheatham, T. E., Darden, T., Gohlke, H., Luo, R., Merz, K. M., et al. (2005). The Amber Biomolecular Simulation Programs. *J. Comput. Chem.* 26, 1668–1688. doi:10.1002/jcc.20290
- Clark, D. E. (2003). In Silico prediction of Blood-Brain Barrier Permeation. *Drug Discov. Today* 8 (20), 927–933. doi:10.1016/s1359-6446(03)02827-7
- Esmailpour, D., Shityakov, S., Tamaddon, A. M., and Bordbar, A. K. (2021). Comparative Chemical Examination of Inclusion Complexes Formed with Beta-Cyclodextrin Derivatives and Basic Amino Acids. *Carbohydr. Polym.* 262, 117868. doi:10.1016/j.carbpol.2021.117868
- Essmann, U., Perera, L., Berkowitz, M. L., Darden, T., Lee, H., and Pedersen, L. G. (1995). A Smooth Particle Mesh Ewald Method. *J. Chem. Phys.* 103, 8577–8593. doi:10.1063/1.470117
- Fu, Z., Aucoin, D., Ahmed, M., Zilio, X., Van Nostrand, W. E., and Smith, S. O. (2014). Capping of Aβeta42 Oligomers by Small Molecular Inhibitors. *Biochemistry* 53 (50), 7893–7903. doi:10.1021/bi500910b
- Gervais, F., Paquette, J., Morissette, C., Krzywkowski, P., Yu, M., Azzi, M., et al. (2007). Targeting Soluble Aβeta Peptide with Tramiprosate for the Treatment of Brain Amyloidosis. *Neurobiol. Aging* 28 (4), 537–547. doi:10.1016/j.neurobiolaging.2006.02.015
- Goodsell, D. S., Morris, G. M., and Olson, A. J. (1996). Automated Docking of Flexible Ligands: Applications of AutoDock. *J. Mol. recognition: JMR* 9 (1), 1–5. doi:10.1002/(sici)1099-1352(199601)9:1<1:aid-jmr241>3.0.co;2-6
- Hou, T., Wang, J., Li, Y., and Wang, W. (2011). Assessing the Performance of the MM/PBSA and MM/GBSA Methods. 1. The Accuracy of Binding Free Energy Calculations Based on Molecular Dynamics Simulations. *J. Chem. Inf. Model.* 51 (1), 69–82. doi:10.1021/ci100275a
- Hritcu, L., Ionita, R., Motei, D. E., Babii, C., Stefan, M., and Mihasan, M. (2017). Nicotine versus 6-Hydroxy-L-Nicotine against Chlorisondamine Induced Memory Impairment and Oxidative Stress in the Rat hippocampus. *Biomed. Pharmacother.* 86, 102–108. doi:10.1016/j.biopha.2016.12.008
- Hubbard, S. J., and Thornton, J. M. (1993). NACCESS. London: Department of Biochemistry and Molecular Biology, University College.
- Kelder, J., Grootenhuys, P. D., Bayada, D. M., Delbressine, L. P., and Ploemen, J. P. (1999). Polar Molecular Surface as a Dominating Determinant for Oral Absorption and Brain Penetration of Drugs. *Pharm. Res.* 16 (10), 1514–1519. doi:10.1023/a:1015040217741
- Khalid, S., Zahid, M. A., Ali, H., Kim, Y. S., and Khan, S. (2018). Biaryl Scaffold-Focused Virtual Screening for Anti-aggregatory and Neuroprotective Effects in Alzheimer's Disease. *BMC Neurosci.* 19 (1), 74. doi:10.1186/s12868-018-0472-6
- Kim, M.-H., Maeng, H. J., Yu, K. H., Lee, K. R., Tsuruo, T., Kim, D. D., et al. (2010). Evidence of Carrier-Mediated Transport in the Penetration of Donepezil into the Rat Brain. *J. Pharm. Sci.* 99 (3), 1548–1566. doi:10.1002/jps.21895
- Kollman, P. A., Massova, I., Reyes, C., Kuhn, B., Huo, S., Chong, L., et al. (2000). Calculating Structures and Free Energies of Complex Molecules: Combining Molecular Mechanics and Continuum Models. *Acc. Chem. Res.* 33, 889–897. doi:10.1021/ar000033j
- Kowal, N. M., Indurthi, D. C., Ahring, P. K., Chebib, M., Olafsdottir, E. S., and Balle, T. (2019). Novel Approach for the Search for Chemical Scaffolds with Activity at Both Acetylcholinesterase and the Alpha 7 Nicotinic Acetylcholine Receptor: A Perspective on Scaffolds with Dual Activity for the Treatment of Neurodegenerative Disorders. *Molecules* 24 (3), 446. doi:10.3390/molecules24030446
- Liu, M., Wan, L., Bin, Y., and Xiang, J. (2017). Role of Norepinephrine in Aβeta-Related Neurotoxicity: Dual Interactions with Tyr10 and SNK(26-28) of Aβeta. *Acta Biochim. Biophys. Sinica* 49 (2), 170–178. doi:10.1093/abbs/gmw126
- Marques, S. M., Šupolíková, L., Molčanová, L., Šmejkal, K., Bednar, D., and Slaninová, I. (2021). Screening of Natural Compounds as P-Glycoprotein Inhibitors against Multidrug Resistance. *Biomedicines* 9 (4), 357. doi:10.3390/biomedicines9040357
- Miyamoto, S., and Kollman, P. A. (1992). Settle: an Analytical Version of the SHAKE and RATTLE Algorithm for Rigid Water Models. *J. Comput. Chem.* 13, 952–962. doi:10.1002/jcc.540130805
- Mok, N. Y., and Brown, N. (2017). Applications of Systematic Molecular Scaffold Enumeration to Enrich Structure-Activity Relationship Information. *J. Chem. Inf. Model.* 57 (1), 27–35. doi:10.1021/acs.jcim.6b00386
- Naghizadeh, S. (2001). castP: Computed Atlas of Surface Topography of Proteins. *Biophysical J.* 80 (1), 320a. doi:10.1366/0003702011953612
- Nie, Q., Du, X. G., and Geng, M. Y. (2011). Small Molecule Inhibitors of Amyloid Beta Peptide Aggregation as a Potential Therapeutic Strategy for Alzheimer's Disease. *Acta pharmacologica Sinica* 32 (5), 545–551. doi:10.1038/aps.2011.14
- Rauk, A. (2008). Why Is the Amyloid Beta Peptide of Alzheimer's Disease Neurotoxic. *Dalton Trans.* 10, 1273–1282. doi:10.1039/b718601k
- Rishton, G. M., LaBonte, K., Williams, A. J., Kassam, K., and Kolovanov, E. (2006). Computational Approaches to the Prediction of Blood-Brain Barrier Permeability: A Comparative Analysis of central Nervous System Drugs versus Secretase Inhibitors for Alzheimer's Disease. *Curr. Opin. Drug Discov. Development* 9 (3), 303–313.
- Shityakov, S., Broscheit, J., and Förster, C. (2012). Alpha-Cyclodextrin Dimer Complexes of Dopamine and Levodopa Derivatives to Assess Drug Delivery to the central Nervous System: ADME and Molecular Docking Studies. *Int. J. nanomedicine* 7, 3211–3219. doi:10.2147/ijn.s31373
- Shityakov, S., Fischer, A., Su, K. P., Hussein, A. A., Dandekar, T., and Broscheit, J. (2020). Novel Approach for Characterizing Propofol Binding Affinities to Serum Albumins from Different Species. *ACS Omega* 5 (40), 25543–25551. doi:10.1021/acsomega.0c01295
- Shityakov, S., and Forster, C. (2014). In Silico predictive Model to Determine Vector-Mediated Transport Properties for the Blood-Brain Barrier Choline Transporter. *Adv. Appl. Bioinform Chem.* 7, 23–36. doi:10.2147/aabc.s63749
- Shityakov, S., Hayashi, K., Störk, S., Scheper, V., Lenarz, T., and Förster, C. Y. (2021). The Conspicuous Link between Ear, Brain and Heart—Could Neurotrophin-Treatment of Age-Related Hearing Loss Help Prevent Alzheimer's Disease and Associated Amyloid Cardiomyopathy. *Biomolecules* 11 (6), 900. doi:10.3390/biom11060900
- Shityakov, S., Roewer, N., Förster, C., and Broscheit, J.-A. (2017). In Silico investigation of Propofol Binding Sites in Human Serum Albumin Using

SUPPLEMENTARY MATERIAL

The Supplementary Material for this article can be found online at: <https://www.frontiersin.org/articles/10.3389/fchem.2021.736509/full#supplementary-material>

- Explicit and Implicit Solvation Models. *Comput. Biol. Chem.* 70, 191–197. doi:10.1016/j.compbiolchem.2017.06.004
- Shityakov, S., Salvador, E., Pastorin, G., and Förster, C. (2015). Blood-brain Barrier Transport Studies, Aggregation, and Molecular Dynamics Simulation of Multiwalled Carbon Nanotube Functionalized with Fluorescein Isothiocyanate. *Int. J. Nanomedicine* 10, 1703–1713. doi:10.2147/ijn.s68429
- Shityakov, S., Sohajda, T., Puskás, I., Roewer, N., Förste, C., and Broscheit, J. A. (2014). Ionization States, Cellular Toxicity and Molecular Modeling Studies of Midazolam Complexed with Trimethyl-Beta-Cyclodextrin. *Molecules* 19 (10), 16861–16876. doi:10.3390/molecules191016861
- Takahashi, R. H., Nagao, T., and Gouras, G. K. (2017). Plaque Formation and the Intraneuronal Accumulation of Beta-Amyloid in Alzheimer's Disease. *Pathol. Int.* 67 (4), 185–193. doi:10.1111/pin.12520
- Vainio, M. J., Kogej, T., Raubacher, F., and Sadowski, J. (2013). Scaffold Hopping by Fragment Replacement. *J. Chem. Inf. Model.* 53 (7), 1825–1835. doi:10.1021/ci4001019
- Voicu, A., Duteanu, N., Voicu, M., Vlad, D., and Dumitrascu, V. (2020). The Rcdk and Cluster R Packages Applied to Drug Candidate Selection. *J. cheminformatics* 12 (1), 3. doi:10.1186/s13321-019-0405-0
- Wallace, A. C., Laskowski, R. A., and Thornton, J. M. (1995). Ligplot - a Program to Generate Schematic Diagrams of Protein Ligand Interactions. *Protein Eng.* 8 (2), 127–134. doi:10.1093/protein/8.2.127
- Walti, M. A., Ravotti, F., Arai, H., Glabe, C. G., Wall, J. S., Böckmann, A., et al. (2016). Atomic-resolution Structure of a Disease-Relevant Aβ(1-42) Amyloid Fibril. *Proc. Natl. Acad. Sci. United States America* 113 (34), E4976–E4984. doi:10.1073/pnas.1600749113
- Wang, W. W., Xu, P., and Tang, H. (2015). Sustainable Production of Valuable Compound 3-Succinoyl-Pyridine by Genetically Engineering *Pseudomonas Putida* Using the Tobacco Waste. *Scientific Rep.* 5. doi:10.1038/srep16411
- Zhang, Y., Zhao, Y., Wang, Z., Gong, H., Ma, L., Sun, D., et al. (2018). Menadione Sodium Bisulfite Inhibits the Toxic Aggregation of Amyloid-Beta(1-42). *Biochim. Biophys. Acta Gen. subjects* 1862 (10), 2226–2235. doi:10.1016/j.bbagen.2018.07.019

Conflict of Interest: The authors declare that the research was conducted in the absence of any commercial or financial relationships that could be construed as a potential conflict of interest.

Publisher's Note: All claims expressed in this article are solely those of the authors and do not necessarily represent those of their affiliated organizations, or those of the publisher, the editors and the reviewers. Any product that may be evaluated in this article, or claim that may be made by its manufacturer, is not guaranteed or endorsed by the publisher.

Copyright © 2021 Shityakov, Skorb, Förster and Dandekar. This is an open-access article distributed under the terms of the Creative Commons Attribution License (CC BY). The use, distribution or reproduction in other forums is permitted, provided the original author(s) and the copyright owner(s) are credited and that the original publication in this journal is cited, in accordance with accepted academic practice. No use, distribution or reproduction is permitted which does not comply with these terms.